NUMERICAL SIMULATION AROUND AIROFOIL WITH TONAL NOISE GENERATION

Takuji Kurotaki*, Takahiro Sumi and Jun Hiyama*****
* **Aerospace Research and Development Directorate, Japan Aerospace Exploration Agency**
** **Department of Mechanical and Aerospace Engineering, Tottori University, Japan**
*** **Sanko Software Dept. Co., Ltd, Japan**

Keywords: *Subsonic Flow, Tonal noise, Unsteady Flow, LES, CFD*

Abstract

A new numerical simulation approach is applied to the flow around an NACA0015 aerofoil with tonal noise generation including the natural transition on the suction side. The acoustic fields clearly show the radiation of sound waves from just after the trailing edge region. Numerical simulations also capture a separated region at the trailing edge on the pressure side. The linear stability analysis on the pressure side shows the possibility of the existence of T-S waves and the most unstable frequency up to the separation almost coincides with the peak frequency. The power spectrum distribution of stream wise velocity fluctuation clearly indicates that the generation of T-S waves on the pressure side is strongly relevant to the determination mechanism of the selection of peak frequency of the tonal edge noise and that the self-excited feedback mechanism exists between just after the stagnation point at the leading edge and the trailing edge region.

1 Introduction

Recently, high-accuracy and high-resolution finite different schemes are widely used in many applications such as problems of aeroacaustics and the stall of an airfoil and so forth. These flows often require accurate unsteady treatments with turbulence, flow separation and flow compressibility. Direct numerical simulations are seemingly possible only for simple geometries at low Reynolds numbers even in near future. Therefore, less expensive methods such as large eddy simulations (LES) are promising approach for high Reynolds numbers and more complex geometries. However, getting quantitatively acceptable results for these flows are still now challenging.

In a previous paper [1], a new approach is proposed in which LES with ADM (approximate deconvolution model) type approach [2] are combined with the generalized characteristic interface conditions [3] for singular lines in a grid and the generalized Navier-Stokes characteristic boundary conditions. Several numerical results are presented including complicated flow aspects such as the natural transition from laminar to turbulent flow around NACA0012 aerofoil in high Reynolds number region. The so-called 2-D T-S wave and the following amplifying oblique waves are clearly captured. The results of linear stability analysis, which is executed by the Orr-Sommerfeld equation with the averaged flow profiles obtained from the LES, coincide with the results directly obtained from the data of fluctuating velocity of LES.

In this paper, this numerical simulation approach is applied to the flow around an aerofoil with tonal noise generation. Some numerical researches have also been conducted recently [4], [5], however, detailed simulation including transition and turbulent boundary layer is still challenging and the numerical approach where the detailed computation region is confined around the trailing edge and some amount of flow fluctuations at the inflow boundary are introduced is commonly used. Here, numerical simulation is conducted around the whole aerofoil and the transition process on

the suction side is captured without modeling. This approach enables us to evaluate the existence of the acoustic feed-back loop and other fundamental physical aspects of the tonal noise generation process.

2 Numerical Method

In this study, the three-dimensional compressible Navier-Stokes equations are employed as the basic equations. For the flow containing turbulence and transition, ADM type approach originally developed by Stolz et. al. [2] is used. In this method, an approximation to the unfiltered solution is obtained from the filtered solution by the series expansion of deconvolution operator. The effect of smaller scales than the filter width is modeled by a relaxation regularization including a dynamically estimated relaxation parameter.

In practical computations with structured grid, singular points can be frequently found where an abrupt grid change exists. These singularities pose troublesome problems especially when high order and high resolution scheme is applied. An excellent theory was proposed [6], which solves the above singular problem by decomposing a computational domain along a line or surface containing the singular points and by imposing accurate characteristic-based interface conditions at the interface. However, the original theory has limitations on the combination between the adjacent computational coordinate definitions, and these two coordinates have to be the same direction and the same coordinate index. A new generalized theory has been proposed by authors [3] for more flexible coordinate arrangement. This theory is applied to the region around a trailing edge when a flow around an airfoil is solved with a C-type single mesh.

Other aspects such as the computation of spatial derivatives, time integration and boundary conditions are also considered to attain high-accuracy and high-resolution schemes as a whole. The spatial derivatives of the inviscid and viscous flux terms are solved by the optimized 4th order penta-diagonal (OFOP) compact difference scheme suggested by Kim et al. [7] . This scheme maintains penta-diagonal Pade form, and has the maximum spatial resolution, optimizing the dissipation and dispersion errors simultaneously. The spatial discretization in the normal direction to boundaries such as wall, outer boundaries and the characteristic-based interface also keeps the 4th order accuracy with the non-centered differencing. For the time integration, the low storage type of 2-step 4th order low-dissipation and low-dispersion Runge-Kutta (LDDRK) scheme (the first step is a 5-stage scheme and the second step is a 6-stage scheme) proposed by Hu et al. [8], [9] is used. This scheme increases numerical stability in the explicit time integration, and reduces the dissipation and dispersion errors simultaneously. CFL=1 is used throughout this study. For the inflow, outflow and wall boundary conditions, the Navier-Stokes characteristic boundary conditions (NSCBC) extended to the generalized coordinate system by Kim et al. [10], [11] are applied. The forced damping of waves with the sponge method near the outer boundary [12] is also applied combined with the implicit damping through the extension of grid intervals in the direction from body to outer boundary.

3 Results and Discussions

3.1 Experiments and Numerical Conditions

In this study, the flow around the NACA0015 airfoil is considered. The chord length is 0.4 m and the angle of attack is -5 degrees. The three uniform flow velocities are selected as 14.5, 20 and 30 m/s and the corresponding Reynolds numbers under the reference chord length were ranging from about 4×10^5 to 8×10^5.

The corresponding experiments were carried out in a closed-loop, closed-test-section, low turbulence (free stream turbulence < 0.05%) wind tunnel facility at the JAXA Aerodynamics Research Group. The wind tunnel is designed to operate at wind tunnel velocities from 1 to 65 m/s and provides a test section of 550 x 650 mm^2.

The model was horizontally fitted in the test section, completely spanning the wind tunnel section. The schematic diagram of experimental setup is shown in Fig. 1.

Acoustic measurements were conducted by a Brüel&Kjær condenser microphone type 4138. The microphone was placed approximately 10cm behind airfoil on the lower wind tunnel wall to avoid flow interference. It was attached on top of a slim wooden mount, elevating the microphone outside the wind tunnel boundary layer in order to prevent the detection of extraneous noise. Velocity measurements were extracted by use of a single wire hotwire technique.

Flow visualization was also carried out by use of a smoke wire technique. For this purpose a 50μm diameter, constantan wire was placed in the flow, 1.5 cm upstream the trailing edge at approximately 1 mm distance from the airfoil surface. In order to illuminate the flow a thin laser sheet was used.

In these experiments, the tonal noise is observed in these flow velocities and the natural laminar-turbulent transitions are observed on the suction side in the experiments.

For the numerical analysis, the same C-type single meshes are used for each case. The total grid points are about 3.5-million, composed of 1001 points in the circumferential direction, 71 points in the radial direction and 51 points in the span wise direction. The grid points are distributed symmetrically on both upper and lower sides and the number of grids along the surface from the leading edge to the trailing edge is 800 points. The total computational domain extends out 10 chord lengths in the radial direction. The last ten points are used for the forced damping of outgoing and incoming waves with sponge method [12] near the outer boundary.

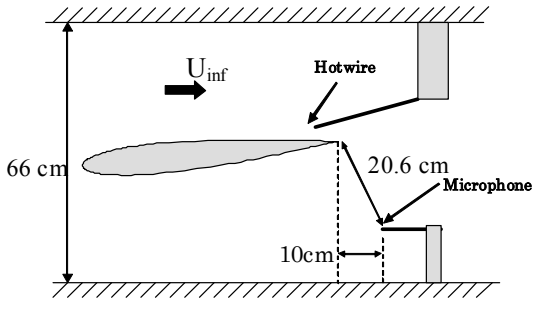

Fig. 1 Schematic diagram of experimental setup.

The span wise length is taken as 0.125 c, where c is the reference chord length. Grid spacing in the radial direction on the wall surface is $2\times10^{-4}c$, which corresponds to less than $\eta^+\approx2$ in wall units in the turbulent boundary layer on the suction side close to the trailing edge for the U_∞ = 14.5 m/s case.

The numerical conditions for each case are summarized in Table 1. The unsteady velocity data in the boundary layer on the pressure side and the pressure data at location corresponding to the microphone are recorded for spectral analysis. Sampling rate is selected as 80 kHz in the dimensional time and the data are collected until the resolution of frequency reaches about 8 Hz.

Table 1 Summary of numerical conditions.

	Case 1	Case 2	Case3
Aerofoil	NACA0015		
Chord length: c	0.4m		
Angle of attack: α	-5 degrees		
Uniform flow velocity: U_∞	14.5 m/s	20 m/s	30 m/s
Reynolds number: Re_∞	4×10^5	6×10^5	8×10^5
Total grid points (circumferential × radial × span wise)	3.6 million (1001 × 71 × 51)		
Spanwise length	0.125 c		
Radial grid spacing on the wall surface	$2\times10^{-4}c$		

3.2 Numerical Results and Comparison with Experiments

In Fig. 2, the frequency/velocity relation is presented for an angle of attack of -5 degrees for both experiments and present CFD. Experimental results show that a ladder like structure with a $U_\infty{}^{1.5}$ trend is observed, consistent to the experiments by Paterson et al [13]. Experiments show that the velocity range for which tonal noise generation occurs is limited from 10 to 32.5 m/s. CFD results also show that the peak frequency is proportional to $U_\infty{}^{1.5}$ and agrees quantitatively well.

The acoustic fields around the airfoil corresponding to each case are captured and evaluated by monitoring the pressure fluctuation directly from CFD results. Fig. 3 shows the instantaneous pressure fluctuation $p-\bar{p}$ around the airfoil at mid-span, where p and $\bar{p}$ denote the instantaneous and averaged pressure respectively. Each figure clearly shows that sound waves are radiating from just after the trailing edge. The wave length of the sound wave changes from about 3 to 1 chord length as the uniform flow velocity increases from 14.5 to 30 m/s.

Fig. 4 shows the frequency spectrum at the location of microphone for each case from the numerical simulation. Sound pressure level at peak frequency is about 90 dB for Case 1, which agrees with the experimental result. CFD results of the peak frequency are at about 270, 440 and 720 Hz respectively for Case 1, 2 and 3, whereas experimental results reveal distinct peaks at 240, 400 and 780 Hz respectively. One of the reasons of these differences of the peak frequencies is that no acoustic lining within a closed-loop, closed-test-section of the wind tunnel facility is applied in the current experimental investigation.

Numerical simulations also capture a separated region at the trailing edge on the pressure side observed in the experiments. Fig. 5 is the change of instantaneous span wise vortex distribution there for Case 1(U_∞ =14.5 m/s). The yellow surface indicates the clockwise direction of span wise vortex and the blue one is the anti-clockwise direction respectively. The corresponding time history of acoustic wave at the microphone is also shown for the reference. These pictures clearly indicate the existence of separating line at about 80% chord length and also show that a small vortex appears just after the separating region and grows gradually and finally collides with the turbulent boundary layer developed on the suction side just after the trailing edge. A small counter rotating vortex also appears at the trailing edge before the collision with the turbulent boundary layer, which is transported downstream in the wake of the large scale eddy. As these vortices are conveyed downstream, the separating region recovers to its initial state. This process is corresponding to one cycle of acoustic waves observed at the place of a microphone.

The same distributions for Case 3(U_∞ =30 m/s) are shown in Fig. 6. The separation region begins after about 80% chord length on the pressure side as the same as Case 1, however, the thickness of the region is smaller. In this case, the span wise nonuniformity appears in the span wise vortex in the separating region, whereas the separating region is almost two dimensional before the collision with the turbulent boundary layer on the suction side in Case 1.

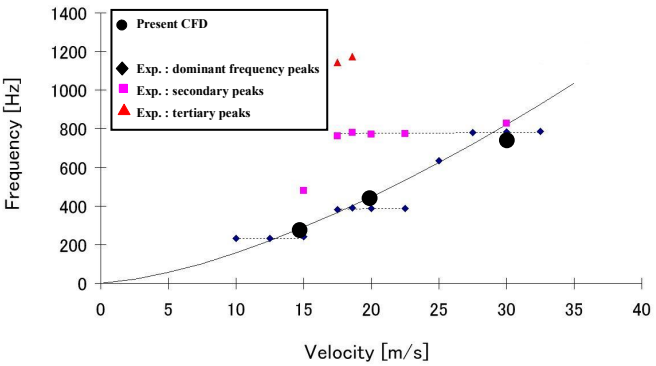

Fig. 2 Velocity/frequency dependency, dotted lines: $U^{0.8}$ dependency, solid line: $U^{1.5}$ dependency.

3.3 Comparison with Linear Stability Analysis

In order to investigate the present results more quantitatively, the linear stability analysis based on the e^N method is conducted. Especially, the possibility of the existence of T-S wave on the pressure side before the separating region and the influence of this T-S wave generation on the self-excited feedback mechanism of the tonal noise are examined. The averaged velocity profile inside the boundary layer directory obtained from the present numerical result is used as input data. In this study, only the numerical results for U_∞= 14.5 m/s, Case 1 is analyzed and characteristics only on the pressure side is treated.

Averaged velocity profiles on the pressure side obtained by the present numerical results at some chord locations are shown in Fig. 7. The horizontal axis is the non-dimensional stream wise velocity normalized by a velocity at the edge of the boundary layer U_e at each *x/c* location and the longitudinal axis is the distance η from the wall normalized by the displacement thickness δ^* of numerical data. These results show the existence of the flow separation near the trailing edge indicated in Fig. 4 and the location of the separation is 82 % chord length for this case.

The linear stability analysis is carried out using these averaged velocity profiles shown in Fig. 5. First of all, how to obtain the N factor, which corresponds to the amplitude of small disturbance propagating inside the boundary layer, is roughly explained here. The amplification rate of the small disturbance at each stream wise location is estimated using the common Orr-Sommerfeld equation,

$$\frac{1}{Re_{\delta^*}}(D^2-\alpha^2)^2\bar{w}+i(\omega-\alpha U)(D^2-\alpha^2)\bar{w}+i\alpha D^2U\bar{w}=0 \quad (1)$$

This equation is derived by the substitution of the following plane wave solution of small disturbance represent as Eq. (2) into the disturbance equation, which is obtained from the basic equation describing the flow field under the two dimensional parallel flow assumption with the unsteady small disturbance,

$$\boldsymbol{u}=\bar{\boldsymbol{u}}(y)\exp\{i(\alpha x-\omega t)\} \quad (2)$$

In Eq. (1) and (2), α denotes a complex wave number, ω a real frequency of the disturbance and U mean velocity in the tangential direction along the surface. $\bar{w}$ is the normalized disturbance of velocity in the orthogonal direction and $\bar{\boldsymbol{u}}(y)$ denotes a vector consists of the small disturbance in the linearized disturbance equations. The growth rate of the disturbance wave depends on the sign of the imaginary part of wave number α_i. Namely, the amplitude of the disturbance wave increases with the increase of x if the sign of the imaginary part of wave number is negative. In other words, the disturbance wave is stable when α_i is positive, and unstable when α_i is negative. Since the disturbance wave develops in the exponential manner under the present assumption, its intensity is usually estimated by e^N method which was proposed by Smith and Gamberoni [14] and Van Ingen [15], and the definition of the N factor is given as following,

$$N\equiv\ln(A/A_0)=-\int_{x_0}^{x_1}\alpha_i dx \quad (3)$$

A_0 denotes the initial amplitude of the disturbance wave at location x_0, and A denotes amplitude at x_1. In general, the laminar-turbulent transition occurs when this N factor reaches to around 12-15 at the location of the corresponding x_1.

In order to calculate the N factor, the complex wave number α at each chord wise location has to be obtained by Eq. (1) as a function of the frequency ω of the disturbance wave. Then integrating the α_i along to x direction, the growth of the N factor is obtained for each frequency. Usually, how define the location x_0 as initial position is an important problem. Here x_0 is defined as the neutral point which corresponds to the position changing the sign of α_i from positive to negative.

Results of the linear stability analysis for disturbance waves with typical frequencies (50-1,400Hz) are shown in Figure 8. Analysis for each frequency is conducted only up to *x/c* = 0.7 because numerical integration of Eq. (3) loses uniqueness due to the emergence of another principal mode attributing the inflection-type instability just before the separation point. It can be seen from this figure that in the leading edge region up to *x/c* = 0.2, the flow is stable and transfers to unstable area where the N factor increases. Furthermore, the critical point, where the stability changes from stable to unstable, moves upstream with the increase of the frequency of the disturbance. These results clearly indicate the possibility of the existence of T-S waves. Up to *x/c* = 0.7, the frequency of the most unstable disturbance exists between 200 and 300Hz. From the N factor distribution as a function of the frequency at the location of *x/c* = 0.7, the most unstable frequency is around 250 Hz which almost coincides with the numerical peak frequency of the tonal edge noise at the location of the microphone as shown in Figure 4 (a).

Fig. 9 is the power spectrum distribution of stream wise velocity fluctuation inside boundary layer on the pressure side for Case 1 directly obtained from the numerical results. The stream wise velocity at 0.64mm distant from the wall surface are analyzed here for the location of x/c = 0.05, 0.2, 0.5 and 0.8. It is noted that at all chord locations, almost the same distributions as the numerical sound frequency spectrum at the location of microphone in Fig. 4 (a) are obtained. Each has the peak at about 270 Hz. This peak value decreases up to x/c = 0.2 and increases up to x/c = 0.8 just before the flow separation. This tendency agrees with the results from the linear stability analysis shown in Figure 8 and the power spectrum distribution at x/c = 0.05 in Fig. 9(a) shows that the influence of the sound generation starts from just after the stagnation region on the pressure side.

The foregoing results clearly indicate that the generation of T-S wave on the pressure side is strongly relevant to the determination mechanism of the selection of peak frequency of the tonal edge noise and that the self-excited feedback mechanism exists between just after the stagnation point at the leading edge and the trailing edge region.

4 Conclusion

In this paper, a new numerical simulation approach for the analysis of subsonic flow is applied to the flow around an aerofoil with tonal noise generation including the natural transition on the suction side. The numerical simulation is conducted around the whole NACA0015 aerofoil and the transition process on the suction side is captured without modeling.

The comparison of the frequency/velocity relation with the corresponding experimental results shows the quantitatively good agreements. The acoustic fields around the airfoil directly from the numerical results clearly show the radiation of sound waves from just after the trailing edge region. The frequency spectrum also show the existence of the peak frequency observed in the experiments although the slight difference exists mainly because of the difference of flow conditions within the closed-loop, closed-test-section of the wind tunnel facility in the experiments.

Numerical simulations also capture a separated region at the trailing edge on the pressure side observed in the experiments. A small vortex appears just after the separating region and grows gradually and finally collides with the turbulent boundary layer developed on the suction side just after the trailing edge. This process is corresponding to one cycle of acoustic waves.

The linear stability analysis on the pressure side with the use of averaged velocity profiles directly calculated numerical results shows the possibility of the existence of T-S waves and the most unstable frequency up to the separation almost coincides with the peak frequency of the tonal noise. The power spectrum distribution of stream wise velocity fluctuation inside the boundary layer on the pressure side from just after the stagnation point to just before the separation line directly obtained from the numerical results shows almost the same distributions as the numerical sound frequency spectrum at the location of microphone. These results clearly indicate that the generation of T-S waves on the pressure side is strongly relevant to the determination mechanism of the selection of peak frequency of the tonal edge noise and that the self-excited feedback mechanism exists between just after the stagnation point at the leading edge and the trailing edge region.

References

[1] Kurotaki, T., Sumi, T. and Atobe, T. Large Eddy Simulation around 2-D Airfoil with Natural Transition at High Reynolds Numpers, ICAS2008-2.1 ST, 2008.

[2] Stolz, S., Adams, N. A., and Kleiser, L. The approximate deconvolution model for LES of compressible flows and its application to shock-turbulent-boundary-layer interaction. *Phys. Fluids*, Vol. 13, pp. 2985-3001, 2001.

[3] Sumi, T., Kurotaki, T.and Hiyama, J. Generalized characteristic interface conditions for high-order multi-block computation. *International Journal of Computational Fluid Dynamics*, Vol. 21, pp. 335-350, 2007.

[4] Wang, M. Computation of Trailing-edge noise at Low Mach number using LES and acoustic analogy, Annual Research Briefs-1998, Center for Turbulence Research, Stanford University/NASA Ames, , pp. 91-106, 1998.
[5] Mathey, F. Computation of Trailing-Edge Noise Using a Zonal RANS-LES Approach and Acoustic Analogy, Conference on Turbulence and Interactions TI2006, 2006.
[6] Kim, J, and Lee, D. Characteristic Interface Conditions for Multiblock High-Order Computation on Singular Structured. Grid. *AIAA Journal*, Vol. 41, pp. 2341-2348, 2003.
[7] J. Kim and D. Lee. Optimized Boundary Compact Finite Difference Schemes for Computational Aeroacoustics, Journal of Computational Physics, Vol. 225,, pp. 995-1019, 2007.
[8] F. Hu, M. Hussaini and J. Manthey. Low-Dissipation and Low-Dispersion Runge-Kutta Schemes for Computational Acoustics. *Journal of Computational Physics*, Vol. 124, pp. 177-191, 1996.
[9] D. Stanescu and W. Habashi. 2N-Storage Low Dissipation and Dispersion Runge-Kutta Schemes for Computational Aeroacoustics. *Journal of Computational Physics*, Vol. 143, pp. 674-681, 1998.
[10] Kim and D. Lee. Generalized Characteristic Boundary Conditions for Computational Aeroacoustics. *AIAA Journal*, Vol. 38, pp. 2040-2049, 2000.
[11] J. Kim and D. Lee. Generalized Characteristic Boundary Conditions for Computational Aeroacoustics, Part 2. *AIAA Journal*, Vol. 42, pp. 47-55, 2000.
[12] T. Colonius. Modeling Artificial Boundary Conditions for Compressible Flow. *Annual Reviews of Fluid Mechanics*, pp. 315-345, 2004.
[13] Paterson, R.W., Vogt, P., Fink, M.R. and Munch, C.L. Vortex noise of Isolated airfoils, J. of Aircraft 10, pp. 296-302, 1973.
[14] Smith, A.M.O. and Gamberoni,N. Transition, Pressure Gradient and Stability Theory. *Douglas Aircraft Co.Rept.* ES 26388, El Segundo, California, 1956.
[15] Van Ingen,J.L. A Suggested Semi-empirical Method for the Calculation of the Boundary Layer Transition Region. *Univ.of Techn.,Dept.of Aero.Eng.Rept.*UTH-74, Delft , 1956.

Copyright Statement

Contact Author Email Address

kurotaki@chofu.jaxa.jp

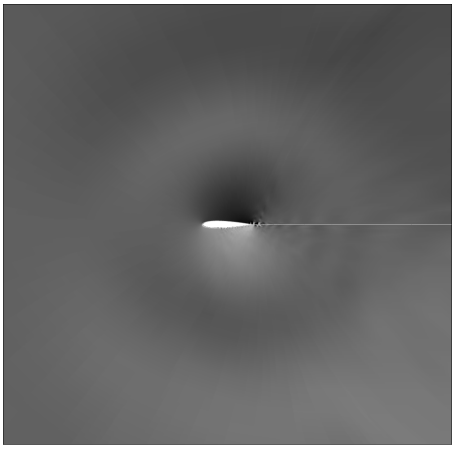

(a) Case 1 (U_∞=14.5 m/s)

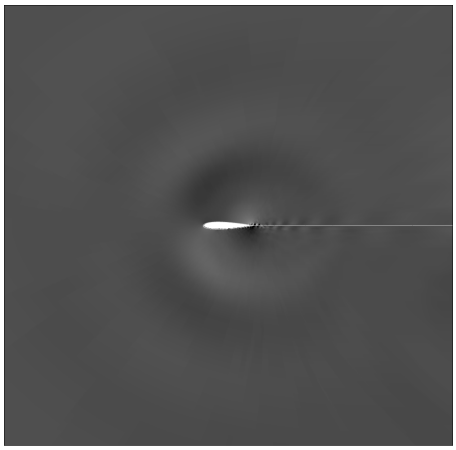

(b) Case 2 (U_∞=20 m/s)

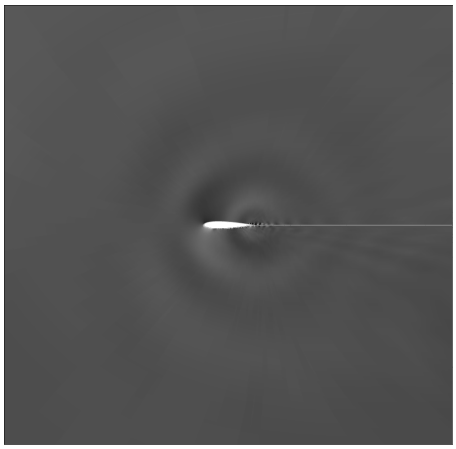

(c) Case 3 (U_∞=30 m/s)

Fig. 3 Instantaneous pressure fluctuation $p-\overline{p}$ around the airfoil at mid-span.

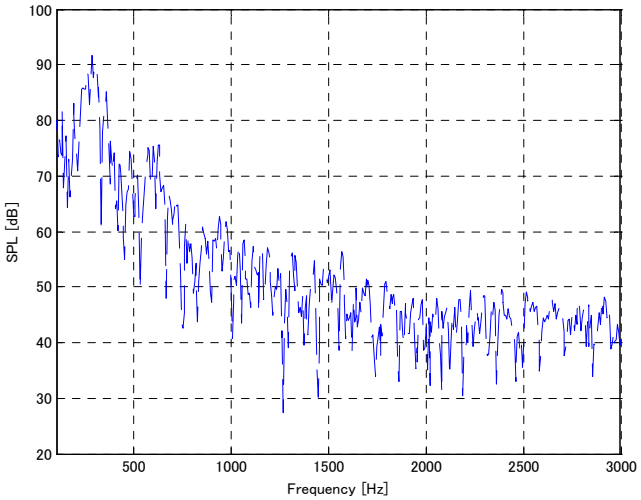

(a) Case 1 (U_∞=14.5 m/s)

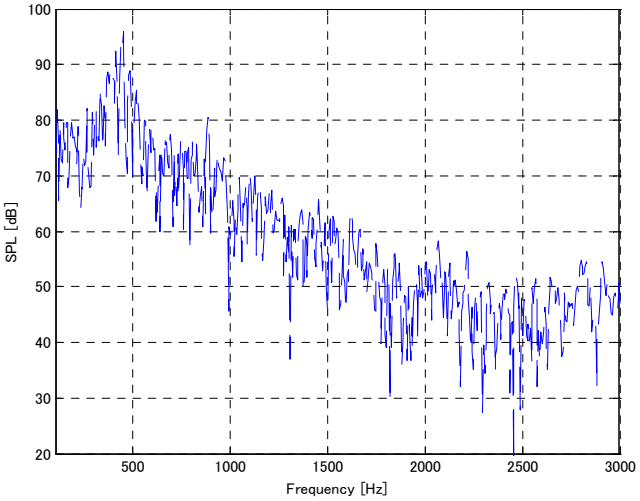

(b) Case 2 (U_∞=20 m/s)

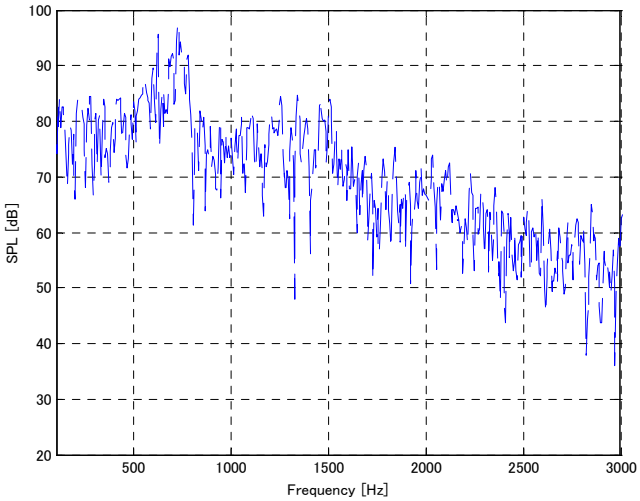

(c) Case 3 (U_∞=30 m/s)

Fig. 4 Frequency spectrum at the location of microphone.

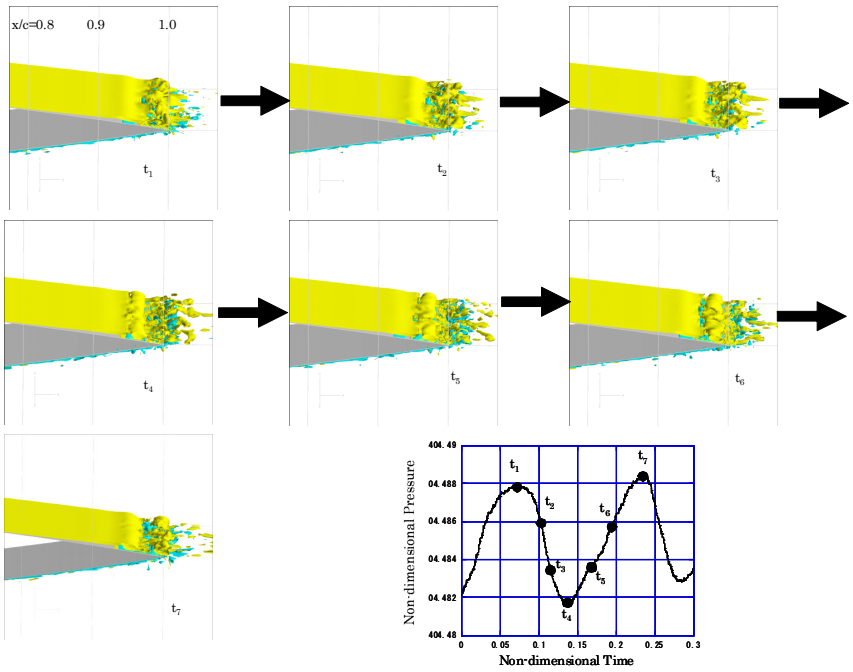

Fig. 5 Change of instantaneous span wise vortex distribution at the trailing edge on the pressure side and corresponding time history of acoustic wave at the microphone (Case 1 ; U_∞=14.5 m/s).

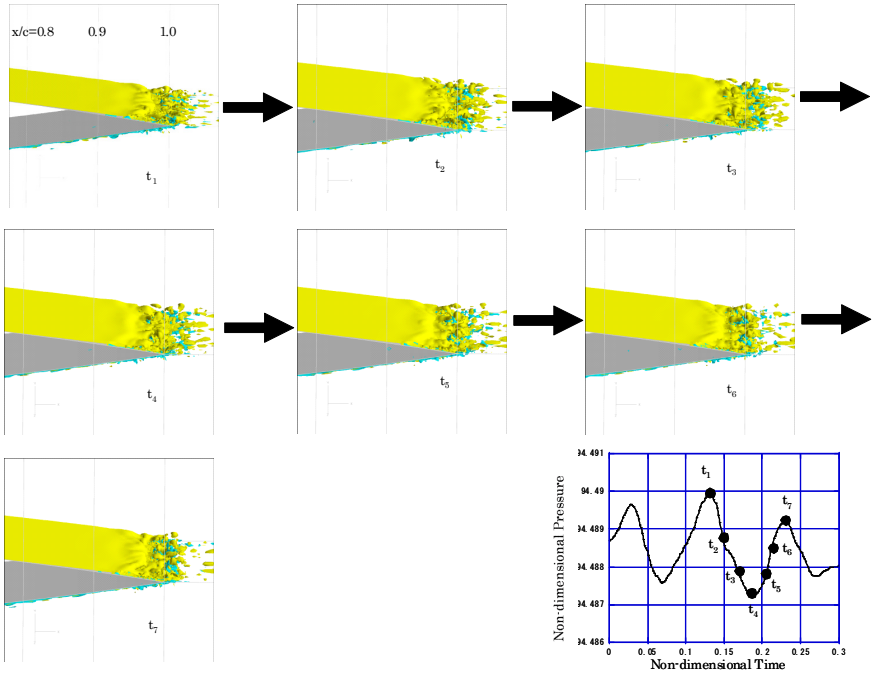

Fig. 6 Change of instantaneous span wise vortex distribution at the trailing edge on the pressure side and corresponding time history of acoustic wave at the microphone (Case 3 ; U_∞=30 m/s).

S

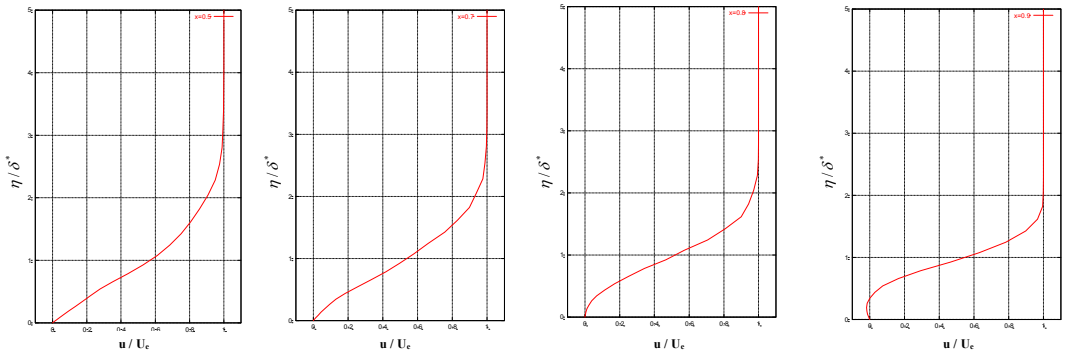

(a) x/c = 0.5 (b) x/c = 0.7 (c) x/c = 0.8 (d) x/c = 0.9

Fig. 7 Averaged velocity profiles on the pressure side at each chord wise location for Case 1 (U=14.5 m/s).

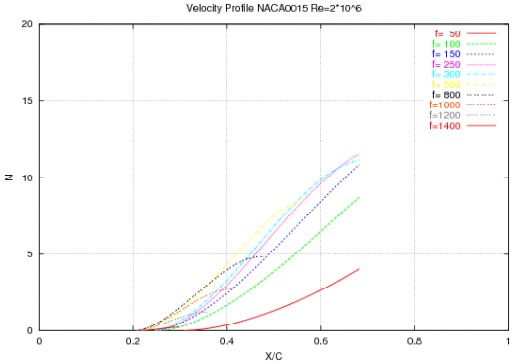

Fig. 8 Variation of N factor with chord wise location x/c for Case 1 (U=14.5 m/s).

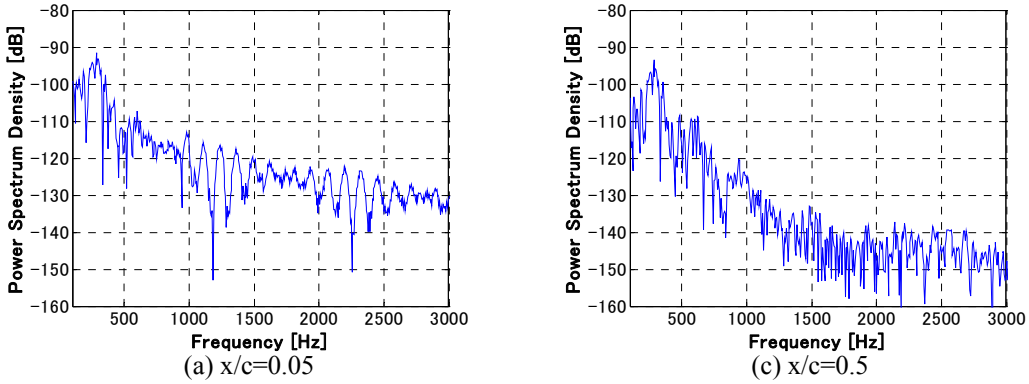

(a) x/c=0.05 (c) x/c=0.5

(b) x/c=0.2 (d) x/c=0.8

Fig. 9. Power spectrum distribution of stream wise velocity fluctuation inside boundary layer at 0.64mm distant from wall surface for Case 1 (U=14.5 m/s).